






Resonant sheath heating in weakly magnetized capacitively coupled plasmas due to electron-cyclotron motion

Quan-Zhi Zhang ^{1,*}, Jing-Yu Sun ^{1,*}, Wen-Qi Lu ^{1,‡}, Julian Schulze ^{1,2}, Yu-Qing Guo,¹ and You-Nian Wang¹

¹Key Laboratory of Materials Modification by Laser, Ion, and Electron Beams (Ministry of Education), School of Physics, Dalian University of Technology, Dalian 116024, China

²Department of Electrical Engineering and Information Science, Ruhr-University, 44780 Bochum, Germany

 (Received 28 October 2020; revised 11 February 2021; accepted 14 September 2021; published 22 October 2021)

An electron heating mechanism based on a resonance between the cyclotron motion of electrons and the radio frequency sheath oscillations is reported in weakly magnetized capacitively coupled plasmas at low pressure. If half of the electron cyclotron period coincides with the radio frequency period, then electrons will coherently collide with the expanding sheath and gain substantial energy, which enhances the plasma density. A relation between the magnetic field and the driving frequency is found to characterize this resonance effect and the kinetics of electrons are revealed at resonance conditions for various driving frequencies.

DOI: [10.1103/PhysRevE.104.045209](https://doi.org/10.1103/PhysRevE.104.045209)

I. INTRODUCTION

Technological high-frequency plasmas represent complex multicomponent and nonlinear systems, whose fundamentals are not understood in many cases. Often such plasmas are magnetized, i.e., an externally applied magnetic field is used to ensure electron confinement and high plasma densities. Despite the lack of fundamental understanding, such plasmas are indispensable tools for a variety of high-technology products of extreme societal relevance such as integrated circuits used for smartphones and laptops [1–3], for biomedical applications such as wound healing and cancer therapy [4–7], as well as for ecological purposes such as gas cleaning and conversion [8,9].

Electron heating mechanisms have long been a central issue in radio frequency (rf) low-temperature plasmas [10–18]. They determine how energy is conveyed from the power supply to the plasma, how the space- and time-dependent electron energy distribution function is shaped, how the discharge is sustained by ionization, and how its characteristics are formed, e.g., radical densities and particle flux-energy distribution functions. In many cases, they are not fully understood. This is particularly true for magnetized plasmas, where complex space- and time-dependent electric and magnetic fields affect the electron dynamics simultaneously. There are two electron heating mechanisms that are considered to be dominant in capacitive rf discharges: (i) Ohmic heating due to electron-neutral collisions and (ii) stochastic heating due to momentum transfer from the oscillating sheaths. However, Schulze *et al.* also proposed the drift-ambipolar heating mechanism, where electrons are accelerated by strong drift and ambipolar electric fields [18–20]. Moreover, resonance

phenomena can occur, at which the power deposition and plasma density will be enhanced, including the plasma series resonance [15], bounce resonance heating [16,17], “striation” resonance mechanism [21].

Most research has been concentrated on the electron heating dynamics in unmagnetized rf discharges and the complex heating mechanisms in magnetized rf discharges have not been addressed adequately. Especially, detailed studies on resonance phenomena in magnetized capacitively coupled rf discharges have not been performed yet to our best knowledge. In electron cyclotron resonance plasmas [22], the frequency of the microwave electric field is chosen to coincide with the cyclotron frequency of electrons in the magnetic field, which greatly enhances the energy coupling efficiency from the microwave power to the plasma. It is, thus, important to explore potential resonance effects and consequences on the electron heating dynamics in magnetized rf discharges, which may facilitate the development of new applications of such discharges.

High ion fluxes toward wafers are often highly desired, as the ion flux, to a large extent, affects the throughput of a given process. The ion flux typically is mostly determined by the plasma density. However, to avoid many ion-neutral collisions inside the sheath and to realize vertical high energy ion bombardment of the wafer in plasma etching, the operation has to be performed at low pressure in real semiconductor industry, which limits the plasma density and the consequent ion flux. Therefore, magnetically enhanced rf plasma sources (so-called rf magnetrons or magnetically enhanced reactive ion etching configurations) are finding increasing interest for sputtering and etching of materials for microelectronics fabrication [1–3,23–26] and fundamental research [27–34]. A transverse static magnetic field approximately parallel to the electrodes is usually applied to confine the light electrons, inducing more ionization or dissociation of the neutral gas and an increased plasma density, while the heavy ions remain unmagnetized due to their much larger Larmor radius,

*These authors contributed equally to this work.

†qzzhang@dlut.edu.cn

‡luwenqi@dlut.edu.cn

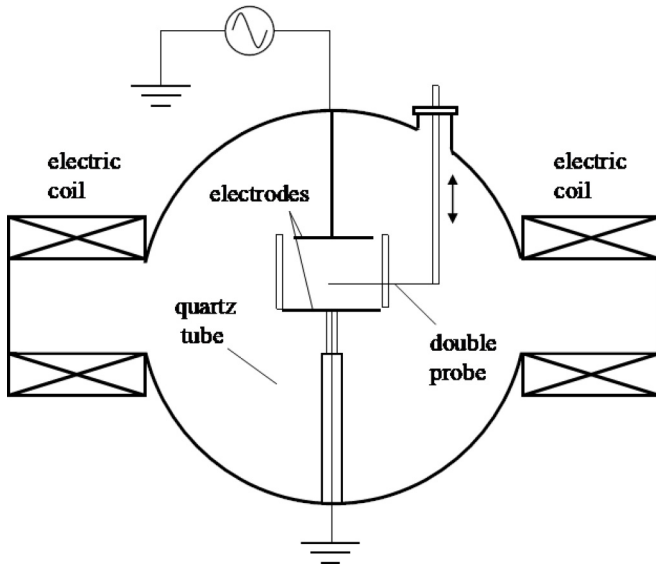


FIG. 1. Schematic plot of the magnetized rf CCP experimental setup.

at a given pressure. Turner *et al.* observed a heating mode transition from a pressure-heating dominated to an Ohmic-heating dominated state induced by a magnetic field in a capacitive rf discharge based on a combination of theoretical model, kinetic simulations and experiments [35]. A relatively comprehensive analysis of magnetized rf discharges has been provided by Lieberman *et al.* Based on a homogeneous sheath model, they qualitatively predicted an enhanced collision-less heating due to potential correlated collisions of electrons with the moving sheath under the effect of the cyclotron motion [36]. However, they did not reveal the inherent physics and the optimal conditions for such an enhancement of the heating rate. A kinetic particle simulation is required to further investigate the complex heating mechanisms in magnetized rf discharges, with the cyclotron motion of electrons considered.

In this paper, we report a resonance effect in magnetized capacitively coupled rf discharges. It is found that if half of the electron cyclotron period coincides with one rf period, then electrons can coherently collide with the expanding rf sheath multiple times at low pressure. In this way, beamlike high energy electrons are produced and cause an increase of the plasma density. As the cyclotron period of electrons is solely determined by the magnetic field, the majority of electrons near the rf sheath edge can experience such a magnetized rf sheath resonance (MRSR) independent of their initial velocity. Our kinetic simulations demonstrate that the MRSR strictly follows a simple relation between the magnetic field and the driving frequency. As a consequence of this resonance, the plasma density is enhanced remarkably for various driving frequencies.

II. EXPERIMENTAL SETUP AND SIMULATION

A. Experimental Setup

A magnetized rf CCP experiment was constructed in a multipurpose setup [37–40], as shown in Fig. 1 below. A stainless steel electrode of 10 cm in diameter was set near the

center of a vacuum chamber, powered by a rf power source of 20 W. A grounded electrode of stainless steel, about 12 cm in diameter, was set below the powered electrode parallel to it. The electrodes were surrounded by a quartz tube of 13.2-cm inner diameter to confine the plasma radially. Two identical coils were installed on opposite sides of the chamber, generating a magnetic field parallel to the electrodes in the discharge region. The discharge is sustained at 0.16 Pa pressure and 4-cm electrode gap in argon gas.

A double probe [41,42] was inserted into the plasma through an aperture in the quartz tube. The tips of the double probe were made of 0.2-mm-thick, 5-mm-long tungsten wires. They were separated by 6 mm and set in the same horizontal plane as the probe, perpendicular to the magnetic field. The probe can be moved vertically to measure the axial distribution of plasma parameters in the radial center of the reactor. There are supposed to be systematic errors for the probe measurements of the plasma density, as the density is deduced based on assumptions from the measured data, and the probe disturbs the plasma around it. However, the reliability of the probe measurements of the plasma density were already verified from the comparison with simulation results in Ref. [41]. We thus do not plot the uncertainties of the probe measurements in this work.

B. Simulation Setup

Our kinetic simulations are based on a 1D3V particle-in-cell (PIC) approach complemented with Monte Carlo treatment of collision (MCC) processes. The code has been benchmarked in Ref. [16]. Important collision processes in argon discharge such as electron-neutral (elastic, inelastic, and ionization) and ion-neutral (elastic and charge exchange) collisions are included in the model. The corresponding cross-section data are taken from Ref. [43]. Our simulations use an explicit scheme, applying a fixed time step 1.6×10^{-11} s for both electrons and ions, and the space-step is set to be around 3.0×10^{-5} m. At least 100 super particles per cell are adopted to satisfy the convergence conditions. The initial electron and ion temperature are set to be 2.0 and 0.026 eV, respectively.

A homogenous magnetic field, B , is applied parallel to the electrodes, which is perpendicular to the electric field. We pay particular attention to the dependence of the plasma density on the externally applied magnetic field for various driving frequencies in argon. The emission of secondary electrons from the electrode surfaces is neglected and the electrodes are assumed to be perfect absorbers of particles for the sake of simplification.

Figure 2 presents the schematic of a geometrically symmetric capacitively coupled rf discharge that is described by our simulation. The lower electrode ($x = 0$) is driven by a single-frequency voltage source (unless specified otherwise, the voltage amplitude is fixed at 300 V), via a blocking capacitor of $C_B = 2$ nF, while the upper electrode is grounded. A spatially homogeneous magnetic field is applied parallel to the electrodes in the y direction, which is perpendicular to the applied electric field in the x direction. The dashed arrows indicate the magnetic field lines. The gap between the electrodes is tuned depending on the discharge conditions. The

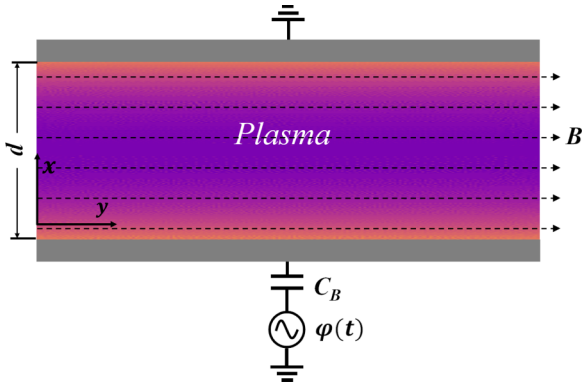


FIG. 2. Schematic plot of the simulation setup for a magnetized rf CCP.

simulation results are verified by probe measurement of the plasma density in a magnetized CCP under similar conditions.

III. RESULTS AND DISCUSSION

Figure 3(a) displays the space- and time-averaged plasma density obtained from the simulations as a function of the externally applied transverse magnetic fields for different driving frequencies and electrode gaps. The plasma density first increases strongly and then decreases with increasing the magnetic field for all frequencies, i.e., a sharp maximum is found at 2.6 G for 13.56 MHz, at 4.8 G for 27.12 MHz, at 8.0 G for 45 MHz, and at 10.8 G for 60 MHz. The formation of these maxima requires a significant enhancement of the electron power absorption and corresponds to a strong change in the discharge properties. This effect is induced by a resonance between the cyclotron motion of electrons and the rf sheath expansion near each electrode, i.e., the MRSR (as explained below). We note that the resonant magnetic field is relatively low at the various driving frequencies, which is beneficial for applications.

In magnetized capacitive rf plasmas, the electrons perform a cyclotron motion, with the cyclotron period of $T_{ce} = \frac{2\pi m_e}{eB}$, where m_e is the electron mass and e is the elementary charge. Meanwhile, the rf sheath oscillates with a period T_{rf} near the electrodes. In this situation, a resonance can be formed between the cyclotron motion of electrons and the rf sheath oscillation based on suitable choices of T_{ce} and T_{rf} . In the absence of collisions and due to the cyclotron motion, electrons accelerated toward the plasma bulk by the expanding sheath will return to this sheath at the following sheath expansion phase if half of T_{ce} corresponds to the rf period. In this way high-energy beam electrons generated by sheath expansion heating will be heated repetitively due to the phase coherence of the electron cyclotron and the sheath motion. Thus, the resonance condition is $0.5T_{ce} = T_{rf}$. Based on this, a relation between the magnetic field B and the driving frequency f_{rf} can be obtained, i.e., $B = \frac{\pi m_e}{e} f_{rf}$, which is plotted in Fig. 3(b). This relation coincides with the magnetic field B required as an input parameter to the PIC or MCC simulation to generate the highest plasma density in Fig. 3(a), indicating a strong resonance effect. As T_{ce} solely depends on the strength of B , the majority of electrons (no matter how fast) near the

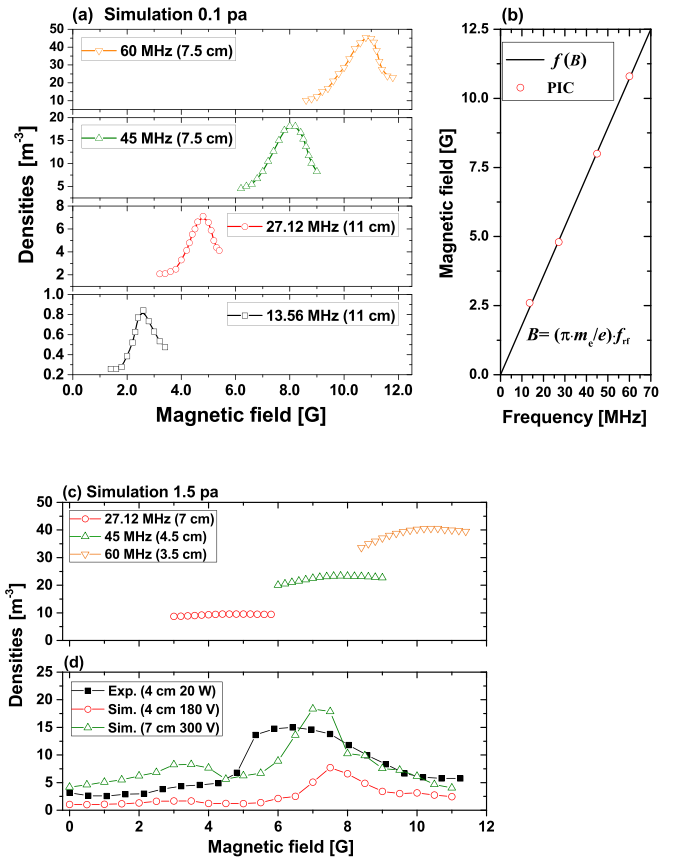


FIG. 3. Space- and time-averaged plasma density (unit in 10^{15} m^{-3}) as a function of the transverse magnetic fields for different frequencies and electrode gaps resulting from PIC simulations at 0.1 Pa (a) and 1.5 Pa (c) for a driving voltage amplitude of 300 V. (b) Externally applied magnetic field at which the highest plasma density is found as a function of the driving frequency obtained from (a) (red points) and from the resonance relation $0.5T_{ce} = T_{rf}$ (solid line). (d) Peak density from experiment at 4-cm gap with 20-W power input, and from PIC simulations for two different electrode gaps of 4 cm with 180-V applied voltage amplitude and 7 cm with 300-V applied voltage amplitudes for 40 MHz at 0.16 Pa.

sheath edges can contribute to the enhancement of the plasma density via the MRSR. This resonance effect has been further verified by experimental measurements performed at two different electrode gaps and shown in Fig. 3(d), which depicts an enhanced density at around 6.5 G in the experiment. This is in qualitative agreement with the density maximums in the simulation. The slight shift of the resonant magnetic field and the broader density profile in the experiment are caused by the nonuniform external magnetic field with a 10–15% lower value at the electrode center, where both the density and magnetic field are measured. The plasma density as a function of the magnetic field is well reproduced qualitatively by the simulations, which validates the used PIC model. In both, experiment and simulation, the plasma density increases by a factor of about 5 at distinct magnetic field strength due to the MRSR. Quantitative agreement between experimental and computational results is not found, i.e., the absolute values of the plasma density obtained from experiment and simulation are not identical, and not to be expected because of the

simplifying assumptions made in the simulation. Our PIC/MCC (i.e., PIC combined with MCC) code is one-dimensional in space and, thus, cannot describe any reactor asymmetry present in the experiment. Moreover, plasma-surface interactions such as secondary electron emission and electron reflection are neglected in the simulation, but are present in the experiment, where they lead to a higher plasma density for 4 cm gap even at low power input. We note that the experiments are performed with small electrodes (~ 10 cm diameter) at low power input. Thus, the magnetic field lines intersect the sidewall. In the experiment, an enhanced electron transport along the magnetic field lines toward the sidewalls happens. Any such effects, which can result in enhanced electron losses to the walls in such a small chamber. In practical manufacturing of integrated circuits, however, the electrode is typically much larger. Usually the electrode diameter is at least 30 cm (with a 30-cm wafer on top) and the reactor wall is located even farther away from the reactor center for state of the art plasma processing applications with much higher power input (i.e., the electrode diameter is much larger than the electrode gap). Thus, the resonant effects are expected to be much stronger in such practical applications. Actually, the much-enhanced plasma density due to MRSR could be beneficial for various low pressure rf plasma applications, such as neutral beam heating of fusion plasma (~ 0.3 Pa) [44] and rf plasma thruster [45] in satellites (~ 0.025 Pa), as it allows to sustain efficient the discharge efficiently at very low pressure.

The resonance effects are further examined at a higher pressure of 1.5 Pa in Fig. 3(c). Although the resonance is attenuated by collisions at higher pressure, it is still substantial at 60 MHz due to the short rf (resonance) period. The collision frequencies for 0.1 Pa and 1.5 Pa are approximately 2.4×10^6 s $^{-1}$ and 3.6×10^7 s $^{-1}$ (the rate coefficient of electron impact collisions in Ar is around 10^{-13} m $^{-3}$ s $^{-1}$ [46]). We can, thus, conclude that the MRSR will occur if the electron impact collision frequency is less than 3.6×10^7 s $^{-1}$ for the studied driving frequencies. The average number of collisions one electron experiences within one rf period is about 0.6 (3.6×10^7 s $^{-1} \times T_{rf} = 0.6$) at 60 MHz and 1.5 Pa. This is less than unity and can serve as a criterion for the MRSR for various gases, pressures, and driving frequencies.

The studied 0.1 Pa is in the pressure range that is relevant for magnetron sputtering applications, in which the pressure is typically lower than 1 Pa to allow collisionless transport of ions and sputtered particles [47], while 1.5 Pa is in the pressure range relevant for plasma etching processes. To realize ever smaller feature sizes (toward 5 nm) and higher aspect ratios of etching trenches, the stable operation of capacitive rf plasmas at high plasma densities is required at lower pressure to realize vertical high ion energy bombardment of the wafer [48]. Until now this has been difficult to achieve. However, the MRSR mechanism might allow to generate a high density discharge at such low pressures and could, thus, be greatly beneficial for advanced plasma processing systems in the semiconductor industry.

Figure 4 shows the trajectory and kinetic energy of a typical resonant electron as well as the position of the sheath edge as a function of time and the temporal evolution of the resonance in the electron $x - v_x$ phase space for 13.56 MHz and 60 MHz, respectively. As revealed in Figs. 4(a) and 4(c),

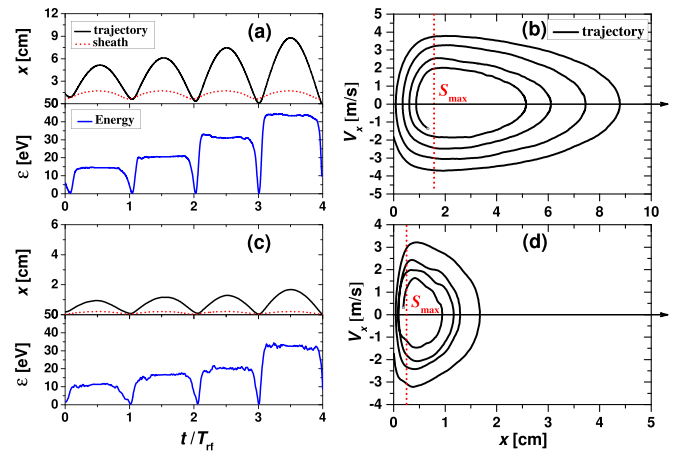


FIG. 4. Position of a typical bouncing electron and of the sheath edge, and the electron kinetic energy as a function of time at (a) 13.56 MHz and (c) 60 MHz. Temporal evolution of the resonance in the electron $x - v_x$ (unit in 10^6 m/s) phase space at (b) 13.56 MHz and (d) 60 MHz. S_{max} are the maximum sheath width.

the electron originating from the expanding sheath repeatedly collides with the sheath during its expansion phase, as the cyclotron motion always returns it back toward the expanding sheath after a time interval of T_{rf} . The electron is first slowed down when entering the expanding sheath and is then accelerated to a higher energy than before on leaving the sheath at each interaction with the oscillating sheath. Its energy remains almost constant during the time the electron spends in the plasma bulk. As a result, it obtains substantial energy during these coherent interactions for both driving frequencies.

As the velocity of electrons is increasing, their spiral trajectories can be revealed in the $x - v_x$ phase space [Figs. 4(b) and 4(d)] due to the increased cyclotron radius. However, as T_{rf} is decreasing toward high driving frequencies and as the cyclotron radius is inversely proportional to B , the magnetic field required to fulfill the resonance condition must be increased as a function of the driving frequency (Fig. 3) and, thus, the distance from the electrode at which the resonant electrons reverse their direction of motion is much smaller at 60 MHz compared to 13.56 MHz, i.e., the electrons are well confined by the resonant B-field near the sheath edge at high frequencies. The resonant electrons may lose energy through inelastic collisions and the phase coherence with the rf sheath oscillation can be lost due to collisions. If the resonant electrons obtain too high energy, then they will overcome the potential barrier in the sheath and will be lost to the electrodes, as can be revealed from Figs. 4(b) and 4(d), where the electrons finally reach the left edge at $x = 0$. This loss mechanism actually results in an upper limit of energy the resonant electrons can gain. In addition, the electrode gap needs to be large enough to allow electrons to gain sufficient energy via the MRSR before they enter the sheath region at the opposite electrode, where their trajectory could be distorted. The minimum electrode gaps could be estimated as 9 cm for 13.56 MHz, 5 cm for 27.12 MHz, 3 cm for 45 MHz, and 2 cm for 60 MHz to produce a strong MRSR based on the x range of resonant electrons shown in Fig. 4, taking the upper limit

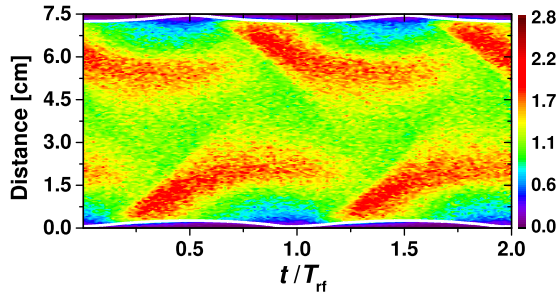


FIG. 5. Spatiotemporal evolution of the electron impact ionization rate (unit in $10^{21} \text{ m}^{-3} \text{ s}^{-1}$) at 60 MHz (contours). The sheath edges are indicated by white lines within two consecutive rf periods.

of 30 eV as reference. The studied electrode gaps are chosen based on these estimations.

To examine the kinetic behavior of electrons in more detail, the spatiotemporally resolved electron impact ionization rate is shown in Fig. 5 for 60 MHz. Beamlike ionization paths with curved profiles are observed near the two electrodes, indicating high energy electron beams. These high energy electron beams originate from the sheath expansion and then return to the sheath due to their cyclotron motion and collide with the expanding sheath coherently. The width of the ionization paths (red color band) is comparable with the variation range of the cyclotron radius (in the bulk) revealed in Fig. 4(d), which suggests that a strong effect of the MRSR is occurring, contributing to the enhanced density shown in Fig. 3. Noting that the variation range of the cyclotron radius (in the bulk) at the resonance conditions of lower driving frequencies is much larger [as revealed from Fig. 4(b)], the ionization paths corresponding to the MRSR would become much broader and even mixed with the ones originating from the opposite expanding sheath. The ionization paths will become vague at low driving frequencies and, thus, we only present the ionization rate for the 60 MHz case.

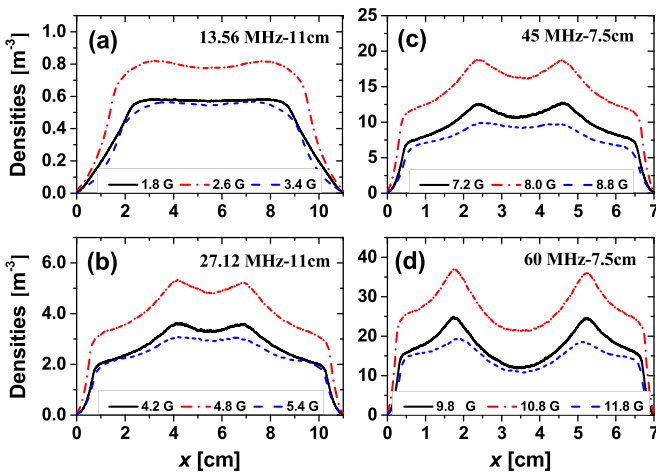


FIG. 6. Time-averaged density (unit in 10^{13} m^{-3}) profiles of high energy electrons ($\geq 30 \text{ eV}$) for different transverse magnetic fields, driving frequencies and electrode gaps: (a) 13.56 MHz at 11 cm, (b) 27.12 MHz at 11 cm, (c) 45 MHz at 7.5 cm, and (d) 60 MHz at 7.5 cm.

The time-averaged density profiles of high energy electrons ($\geq 30 \text{ eV}$) are presented in Fig. 6 for different magnetic fields, driving frequencies and electrode gaps. The high energy electron densities are particularly increased due to the MRSR if the resonance condition is fulfilled. The gyrating electrons gain substantial energy during the repeated collisions with the rf oscillating sheath due to the MRSR. As mentioned above, the variation range of the cyclotron radius at resonant conditions becomes more narrow at higher frequencies, i.e., the confinement effect is strengthened at larger resonant magnetic fields and the high energy electrons tend to be localized near the sheath edges, gradually producing bimodal distributions of their density profile at high frequencies. The generated high energy electrons play a crucial role in enhancing the plasma density via ionization and finally lead to the generation of the peak densities shown in Fig. 3 at resonant conditions.

IV. CONCLUSION

Our kinetic simulations reveal a resonance phenomenon in magnetized capacitively coupled plasmas at low pressure. This resonance effect is also verified experimentally. If half of the electron cyclotron period coincides with the rf period, then electrons will repeatedly collide with the rf oscillating sheath during its expansion phase and, thus, will gain substantial energy. The MRSR strictly follows a resonance condition between the externally applied magnetic field and the driving frequency, which does not depend on the initial velocity of the electrons, which allows the majority of electrons near the rf sheath to be affected by the MRSR. The plasma density can be tremendously enhanced at the resonance conditions for various driving frequencies. The required resonant magnetic field is low, which may be beneficial for applications. The MRSR may not only occur in magnetized capacitively coupled plasmas, but also in other magnetized rf discharges with regularly oscillating sheaths. This effect is expected to be highly relevant to both fundamental and applied plasma science. In fact, it helps to understand the electron heating dynamics in low pressure magnetized rf capacitively coupled plasmas and may promote the industrial applications of magnetized low temperature plasmas in semiconductor fabrication, where the MRSR can be used to control the plasma and to tailor plasma parameters.

Note added in proof. Similar work has recently come to our attention, in which an enhanced operational regime for high-frequency capacitive discharges in the presence of a weak magnetic field is also found by Patil *et al.* [49].

ACKNOWLEDGMENTS

This work is financially supported by the National Natural Science Foundation of China (NSFC) (Grants No. 11935005 and No. 12020101005), the Fundamental Research Funds for the Central Universities (Grants No. DUT18TD06 and No. DUT20LAB201), the Scientific Research Foundation from Dalian University of Technology [Grant No. DUT19RC(3)045], and the German Research Foundation in the frame of the project “Plasmabasierte Prozessfuehrung von reaktiven Sputterprozessen” (No. 417888799).

- [1] W. P. Leroy, S. Mahieu, D. Depla, and A. P. Ehiasarian, *J. Vac. Sci. Technol. A* **28**, 108 (2010).
- [2] V. M. Donnelly and A. Kornblit, *J. Vac. Sci. Technol. A* **31**, 050825 (2013).
- [3] X. Tian, Y. Ma, J. Hu, M. Bi, C. Gong, and P. K. Chu, *J. Vac. Sci. Technol. A* **35**, 021402 (2017).
- [4] W. Jiang, J. Tang, Y. Wang, W. Zhao, and Y. Duan, *Appl. Phys. Lett.* **104**, 013505 (2014).
- [5] R. Safari and F. Sohbatzadeh, *Ind. J. Phys.* **89**, 495 (2015).
- [6] N. Eswaramoorthy and D. R. McKenzie, *Biophys Rev.* **9**, 895 (2017).
- [7] C. Y. T. Tschang, R. Bergert, S. Mitic, and M. Thoma, *J. Phys. D* **53**, 215202 (2020).
- [8] R. Snoeckx and A. Bogaerts, *Chem. Soc. Rev.* **46**, 5805 (2017).
- [9] R. Brandenburg, A. Bogaerts, W. Bongers, A. Fridman, G. Fridman, B. R. Locke, V. Miller, S. Reuter, M. Schiorlin, T. Verreycken, and K. K. Ostrikov, *Plasma Process. Polym.* **16**, 1700238 (2019).
- [10] M. M. Turner, *Phys. Rev. Lett.* **75**, 1312 (1995).
- [11] G. Gozadinos, M. M. Turner, and D. Vender, *Phys. Rev. Lett.* **87**, 135004 (2001).
- [12] M. M. Turner, *J. Phys. D: Appl. Phys.* **42**, 194008 (2009).
- [13] B. P. Cluggish, J. R. Danielson, and C. F. Driscoll, *Phys. Rev. Lett.* **81**, 353 (1998).
- [14] J. Schulze, B. G. Heil, D. Luggenhölscher, R. P. Brinkmann, and U. Czarnetzki, *J. Phys. D* **41**, 195212 (2008).
- [15] T. Mussenbrock, R. P. Brinkmann, M. A. Lieberman, A. J. Lichtenberg, and E. Kawamura, *Phys. Rev. Lett.* **101**, 085004 (2008).
- [16] Y. X. Liu, Q. Z. Zhang, W. Jiang, L. J. Hou, X. Z. Jiang, W. Q. Lu, and Y. N. Wang, *Phys. Rev. Lett.* **107**, 055002 (2011).
- [17] Y. X. Liu, Q. Z. Zhang, W. Jiang, W. Q. Lu, and Y. N. Wang, *Plasma Sources Sci. Technol.* **21**, 035010 (2012).
- [18] J. Schulze, A. Derzsi, K. Dittmann, T. Hemke, J. Meichsner, and Z. Donkó, *Phys. Rev. Lett.* **107**, 275001 (2011).
- [19] J. Schulze, Z. Donkó, A. Derzsi, I. Korolov, and E. Schuengel, *Plasma Sources Sci. Technol.* **24**, 015019 (2015).
- [20] J. Schulze, Z. Donkó, T. Lafleur, S. Wilczek, and R. P. Brinkmann, *Plasma Sources Sci. Technol.* **27**, 055010 (2018).
- [21] Y. X. Liu, E. Schüngel, I. Korolov, Z. Donkó, Y. N. Wang, and J. Schulze, *Phys. Rev. Lett.* **116**, 255002 (2016).
- [22] H. Conrads and M. Schmidt, *Plasma Sources Sci. Technol.* **9**, 441 (2000).
- [23] K. E. Davies, M. Gross, and C. M. Horwitz, *J. Vac. Sci. Technol. A* **11**, 2752 (1993).
- [24] G. F. McLane and J. R. Flemish, *Appl. Phys. Lett.* **68**, 3755 (1996).
- [25] R. A. Lindley, C. H. Björkman, H. Shan, K.-H. Ke, K. Doan, R. R. Mett, and M. Welch, *J. Vac. Sci. Technol. A* **16**, 1600 (1998).
- [26] C. T. Gabriel, *J. Vac. Sci. Technol. B* **20**, 1542 (2002).
- [27] D. A. Hutchinson, M. M. Turner, R. A. Doyle, and M. B. Hopkins, *IEEE Trans. Plasma Sci.* **23**, 636 (1995).
- [28] D. J. Helfritsch, in *Proceedings of the IEEE Transactions on Industry Applications* (IEEE, Los Alamitos, CA, 1993), Vol. 29, pp. 882–886.
- [29] J. C. Park and B. Kang, *IEEE Trans. Plasma Sci.* **25**, 499 (1997).
- [30] M. J. Kushner, *J. Appl. Phys.* **94**, 1436 (2003).
- [31] Y. Yang and M. J. Kushner, *J. Vac. Sci. Technol. A* **25**, 1420 (2007).
- [32] S. Yang, Y. Zhang, H. Y. Wang, S. Wang, and W. Jiang, *Plasma Sources Sci. Technol.* **26**, 065011 (2017).
- [33] M. Oberberg, J. Kallahn, P. Awakowicz, and J. Schulze, *Plasma Sources Sci. Technol.* **27**, 105018 (2018).
- [34] M. Oberberg, D. Engel, B. Berger, C. Wölfel, D. Eremin, J. Lunze, R. P. Brinkmann, P. Awakowicz, and J. Schulze, *Plasma Sources Sci. Technol.* **28**, 115021 (2019).
- [35] M. M. Turner, D. A. W. Hutchinson, R. A. Doyle, and M. B. Hopkins, *Phys. Rev. Lett.* **76**, 2069 (1996).
- [36] S. E. Savas and A. J. Lichtenberg, *IEEE Trans. Plasma Sci.* **19**, 189 (1991).
- [37] J. Xu, X. Deng, J. Zhang, W. Lu, and T. Ma, *Thin Solid Films* **390**, 107 (2001).
- [38] X. Jun, D. Xinlu, Y. Shiji, L. Wenqi, and M. Tengcai, *J. Vac. Sci. Technol. A* **19**, 425 (2001).
- [39] J.-Q. Li, J. Xu, Y.-J. Bai, W.-Q. Lu, and Y.-N. Wang, *J. Vac. Sci. Technol. A* **34**, 061304 (2016).
- [40] Y.-J. Bai, W.-Q. Lu, J.-Q. Li, J. Xu, and Y.-N. Wang, *Phys. Plasmas* **23**, 083522 (2016).
- [41] L. Wenqi, J. Xiangzhan, L. Yongxin, Y. Shuo, Z. Quanzhi, L. Xiaosong, X. Yong, Z. Aimin, and W. Younian, *Plasma Sci. Technol.* **15**, 511 (2013).
- [42] X.-Z. Jiang, Y.-X. Liu, S. Yang, W.-Q. Lu, Z.-H. Bi, X.-S. Li, and Y.-N. Wang, *J. Vac. Sci. Technol. A* **29**, 011006 (2011).
- [43] V. Vahedi and M. Surendra, *Comput. Phys. Commun.* **87**, 179 (1995).
- [44] D. Wunderlich, S. Mochalsky, U. Fantz, P. Franzen, and the NNBI-Team, *Plasma Sources Sci. Technol.* **23**, 015008 (2014).
- [45] K. Takahashi, *Sci. Rep.* **11**, 2768 (2021).
- [46] M. A. Lieberman and A. J. Lichtenberg, *Principles of Plasma Discharges and Materials Processing* (John Wiley & Sons, New York, 2005).
- [47] R. Hollerweger, D. Holec, J. Paulitsch, R. Rachbauer, P. Polcik, and P. H. Mayrhofer, *J. Phys. D* **46**, 335203 (2013).
- [48] M. Kulsreshath, A. Vital, P. Lefauchaux, C. Sinturel, T. Tillocher, M. Vayer, M. Boufnichel, and R. Dussart, *Micro Nano Eng.* **1**, 42 (2018).
- [49] S. Patil, S. Sharma, S. Sengupta, A. Sen, and I. Kaganovich, An enhanced operating regime for high frequency capacitive discharges, [arXiv:2012.02752](https://arxiv.org/abs/2012.02752) (2020).